TOPOGRAPHIC ROUGHNESS AND PHYSICAL MODELS OF TEXTURE FORMATION ON THE NORTH POLAR RESIDUAL CAP OF MARS. P. O. Hayne[1] and A. X. Wilcoski[1], [1]Laboratory for Atmospheric and Space Physics, University of Colorado Boulder (Paul.Hayne@Colorado.edu).

Introduction: Mars' north polar residual cap (NPRC) is a perennial layer of H_2O ice that was likely emplaced near the end of the ~5-Myr period of secular obliquity variations driving accumulation of the underlying north polar layered deposits (NPLD) [1]. Surface age estimates of the NPRC based on crater counts span ~1 to 10 kyr [2, 3], with the dominant uncertainties coming from the crater production function, mechanical properties of the target material, and the nature of the processes responsible for erasing craters on the icy surface.

In addition to the relatively few detectable craters, the surface texture of the NPRC appears heavily-eroded, with regularly spaced topography sometimes exhibiting linear, pitted, or polygonal patterns with characteristic scales of order 10 m [4, 5, 6]. Thermal- and near-IR measurements of the NPRC are consistent with relatively high thermal inertia [7] and large H_2O ice grain sizes [8], suggesting relatively old ice. However, fundamental questions remain regarding the formation and subsequent modification of the NPRC, including the basic question of whether it currently exists in a state of net accumulation or alternatively, ablation.

A previous study [9] developed an insolation-driven model of NPRC surface evolution, which was able to reproduce the dominant topographic wavelengths after a few kyr. Here, we combine a more detailed statistical analysis of high-resolution surface topography data with physics-based ablation/accumulation models to better constrain the NPRC mass balance and age. We also use the derived roughness statistics to predict lander-scale slopes relevant to future missions to Mars' polar regions.

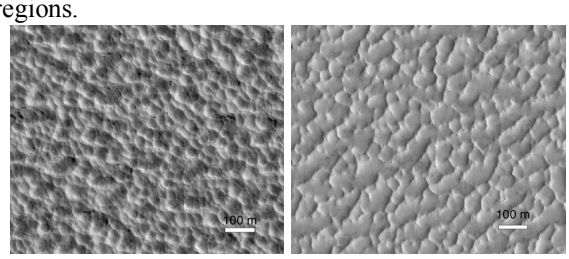

Figure 1: Surface textures of the north polar residual cap (NPRC) from HiRISE image frames ESP_001922_2680 (left) at (135.1°E, 87.9°N) and ESP_045346_2680 (right) at (120.7°E, 87.8°N). The scale bars indicate 100 m, and illumination is approximately from the right in both images, which have a resolution of ~30 cm/pixel.

Dataset: We used publicly available images and digital terrain models (DTMs) from the High Resolution Imaging Science Experiment (HiRISE, [10]) on NASA's Mars Reconnaissance Orbiter. Images selected for this study contained regions of the upper surface of the NPRC acquired during northern summer (in the range L_S = 100° – 150°) when all seasonal frost had disappeared. Whereas the HiRISE images had typical spatial resolution ~25 cm/pixel, the standard DTMs had sampling at ~1 m/pixel.

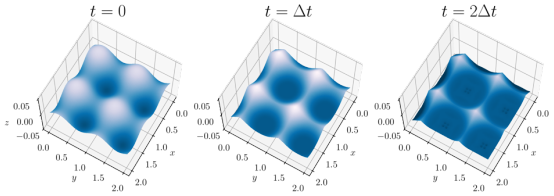

Figure 2: Modeled 3-d surface evolution during insolation-dominated ice ablation. Frames are shown for the initial state ($t = 0$) and two later times at equal increments, with arbitrary spatial scale. Starting with an initially sinusoidally varying surface, the increase in concavity is entirely due to differential solar absorption by sloped surfaces in this model.

Surface Roughness Statistics: Relevant statistical measures of surface roughness and topographic modes were calculated for the 2-d elevation profiles extracted from the DTMs. Here, we focus on: 1) the correlation length, ξ, which relates to the horizontal scale of spatially repeating features, and 2) the Hurst exponent, H, which defines the degree of self-similarity of the surface over a given range of spatial scales. The correlation length (also called the structure function [Aharonson06]) is related to the dominant topographic wavelength through $\lambda \sim 3\xi$, and is found through fitting the autocorrelation vs. displacement Δx with a function $g(\Delta x) = Ce^{-(\Delta x/\xi)^{2H}}$ [11]. The Hurst exponent is calculated from $m(\Delta x) = m(\Delta x_0)(\Delta x/\Delta x_0)^{H-1}$, where m is the root mean square (RMS) slope with horizontal resolution L. Since RMS slope is a measure of surface roughness at a given scale, the Hurst exponent provides a measure of the change in roughness with changing scale [12, 13].

Concavity of the surfaces can be quantified using the mean of the second derivative of height for collections of points $z_i = z(x_i)$ along horizontal profiles with

distances x_i. With $z'' = \partial^2 z/\partial x^2$, we used the metric $C_N = \frac{1}{\sigma}\langle z'' \rangle_N > 1$ where σ is the standard deviation of z'' for the collection of N points. The concavity metric can be evaluated for different choices of the spacing Δx in $\{x_i\}$, and the parameter C_N can be evaluated at $\Delta x \sim \lambda$, close to the dominant topographic wavelength.

Ablation/accumulation Model: Simulations of rough surface evolution through both accumulation and ablation of ice were performed using a numerical model including atmospheric effects, surface-to-surface radiative transfer, shadowing, and subsurface heat transfer [9]. In this work, we further explore the surface evolution through comparison to the measured roughness statistics of the NPRC, and also incorporate a 3-d surface evolution model based on terrestrial ablation hollows ("suncups") formation [14]. The latter includes the effects of differential absorption and emission of radiation on each surface element of a curved surface, due to both solar incidence-angle dependent multiple-scattering within the ice [15] and the reduction sky view on the walls of such features.

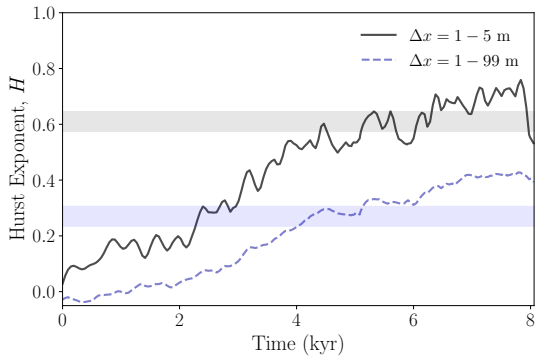

Figure 3: Time-evolution of the Hurst exponent, H, in the 2-d rough-surface model, for a 100-m long surface with horizontal resolution of 25 cm at 85°N.

Results: Across the 5 DTMs analyzed, we find consistent values for the correlation length, $\xi \approx 5 - 10$ m, or $\lambda \approx 15 - 30$ m, consistent with previous results [4, 5, 6]. Similarly, the Hurst exponent is consistently $H \approx 0.6$ for $\Delta x = 1 - 5$ m, and $H \approx 0.25$ for $\Delta x = 1 - 100$ m. These results indicate the strong dominance of the ~10-m scale roughness over other wavelengths, and are consistent with the relative shallowing of slopes at scales smaller than 10 m, based on the abrupt decrease in surface roughness (i.e., larger H for $\Delta x < 10$ m).

Comparing the data to the models, we find that the pitted surface topography observed on the NPRC is dominated by concave features similar in morphology to modeled ablation hollows (cf. Figs. 1 & 2). The concavity parameter for the surfaces in Figure 1 is $C_N > 1$ for collections of $N > 100$ points, indicating topography dominated by concave features. In fact, the resulting concave geometry is a natural consequence of insolation-dominated ablation of snow and ice, often observed at high altitudes on Earth [16]. Surface roughness evolution from the 2-d model is also consistent with the data: measured values of ξ and H are achieved after ~4 kyr and ~5 kyr of model evolution, respectively (Fig. 3).

Discussion: A key result of previous modeling work [9] is that ablation and accumulation both lead to similar changes in the surface roughness and dominant topographic wavelength of the NPRC. It was therefore unclear how to distinguish between these two regimes and interpret the mass balance (and therefore climatic state) of the NPRC. However, the high-resolution images and DTMs analyzed here may be more consistent with surface evolution primarily due to ablation, for two reasons: 1) differential growth of slopes occurs in the model primarily during summertime, when ablation should dominate; 2) the concavity of the dominant topographic features is readily explained by insolation-driven ablation, and cannot be easily explained by accumulation. Furthermore, independent observations suggest a surface composed of large-grained, relatively coherent ice, consistent with ablation rather than recent or ongoing net accumulation [7, 8]. If borne out by additional observations and models, these results suggest that the NPRC is presently undergoing net removal, perhaps indicating a reversal in the climate state that led to the initial deposition of the NPLD.

Acknowledgments: Part of this work was supported by the NASA Mars Reconnaissance Orbiter project. Data used in this study can be found on the NASA Planetary Data System Imaging Node: https://pds-imaging.jpl.nasa.gov/

References: [1] Smith I. B. et al. (2020) *Planet. Space Sci., 184,* 104841. [2] Banks M. E. et al. (2010) *JGR,* 115(E8). [3] Landis M. E. et al. (2016) *GRL, 43*(7) 3060-3068. [4] Milkovich S. M. and Head J. W. (2006) *Mars, 2,* 21-45. [5] Parra S. A. et al. (2017) *LPSC, 1964*, 1719. [6] Russell P. S. et al. (2019) *LPSC, 2132*, 3048. [7] Bapst J. et al. (2019) *JGR*, *124* 1315-1330. [8] Langevin Y. et al. (2005) *Science, 307*, 1581-1584. [9] Wilcoski A. X. and Hayne P. O. (2020) *JGR, 125*, 12. [10] McEwen A. S. et al. (2007), *JGR*, *112*(E5). [11] Labat S. C. et al. (2002) *Appl. Surf. Sci.*, *188*, 182-187. [12] Aharonson O. and Schorghofer N. (2006) *JGR, 111*(E11). [13] Gerekos C. et al. (2021) *Icarus*, *358*, 114197. [14] Tiedje, T. et al. (2006) *JGR*, *111*(F2). [15] Wiscombe W. J. and Warren S. G. (1980) *J. Atmos. Sci.*, *37*(12). [16] Betterton M. D. (2001) *Phys. Rev. E.*, *63*(5).